The importance of an external circuit in a particle-in-cell/Monte Carlo collisions model for a direct current planar magnetron

E. Bultinck,[1,a)] I. Kolev,[1] A. Bogaerts,[1] and D. Depla[2]
[1]*Research Group PLASMANT, Department of Chemistry, University of Antwerp, Universiteitsplein 1, 2610 Antwerp, Belgium*
[2]*Department of Solid State Sciences, Ghent University, Krijgslaan 281 (S1), 9000 Ghent, Belgium*

(Received 17 May 2007; accepted 31 October 2007; published online 14 January 2008)

In modeling direct current (dc) discharges, such as dc magnetrons, a current-limiting device is often neglected. In this study, it is shown that an external circuit consisting of a voltage source and a resistor is inevitable in calculating the correct cathode current. Avoiding the external circuit can cause the current to converge (if at all) to a wrong volt-ampere regime. The importance of this external circuit is studied by comparing the results with those of a model without current-limiting device. For this purpose, a 2d3v particle-in-cell/Monte Carlo collisions model was applied to calculate discharge characteristics, such as cathode potential and current, particle fluxes and densities, and potential distribution in the plasma. It is shown that the calculated cathode current is several orders of magnitude lower when an external circuit is omitted, leading to lower charged particle fluxes and densities, and a wider plasma sheath. Also, it was shown, that only simulations with external circuit can bring the cathode current into a certain plasma regime, which has its own typical properties. In this work, the normal and abnormal regimes were studied. © *2008 American Institute of Physics*. [DOI: 10.1063/1.2828155]

I. INTRODUCTION

Magnetron discharges play a very important role for the sputter deposition of thin films since the early 1970s.[1] Currently, magnetrons are the most important tools for industrial sputter deposition of thin metallic or nonmetallic coatings. In a magnetron reactor, the magnet, with a typical maximum B-field strength of 0.02−0.1 T,[2] is placed behind the cathode. This causes the electrons to be trapped near the cathode surface, resulting in an enhanced ionization of the background gas. This results in a very efficient sputtering process and allows the magnetron to operate at lower pressures (typically in the range of 0.1–1 Pa)[2] in comparison to nonmagnetized sputtering discharges. Due to the lower pressure, the sputtered atoms will be less scattered on their way to the substrate. This results in a more efficient deposition. Different magnetic configurations exist. A frequently used one is a planar magnetron, which can be rectangular or circular. The magnetron we modeled is a planar circular magnetron.

To improve the applications of magnetron sputter deposition of thin films, a good insight in the magnetron discharge behavior is desirable. This can be acquired by plasma diagnostics such as probe measurements and by numerical simulations. Different kinds of models can be applied to simulate gas discharges, such as continuum and particle models. Because of the low pressure of magnetron discharges, the continuum model does not describe the plasma very accurately. Also, the complexity of the magnetic field makes a continuum model very inefficient.[3] To overcome these obstacles, the so-called particle-in-cell/Monte Carlo collisions (PIC/MCC) model is more suitable.

The PIC/MCC method is a self-consistent modeling approach. The particles move in the electric and magnetic fields according to Newton's law. Their collisions are described in the MCC module and their interaction with the walls is also treated. Afterwards, new positions and velocities are calculated. The particle positions are first-order weighted to the grid on which the Poisson equation is solved to calculate the potential and the electric field. This new electric field moves the particles again. In contrast to the electric field, the magnetic field generated by the particles does not perturb the strong applied magnetic field. In other words, the magnetic field in the chamber is assumed to be equal to the external magnetic field.

In the existing PIC/MCC models for direct current (dc) discharges a so-called external circuit, which acts as current-limiting device, is often neglected (among which in magnetrons[4–6]). Without a current-limiting device, the cathode current may converge (if it converges at all) to a wrong volt-ampere regime what makes it impossible to validate the calculated cathode current with experimental values. Moreover, this leads to an incorrect prediction of the plasma characteristics. In Refs. 4 and 5, nothing is mentioned about convergence of the cathode current at all, and in Ref. 6, the authors conquered convergence problems which they solved by trial and error of different input parameters such as voltage, pressure, and secondary electron emission coefficient. In both cases, the cathode current was not verified with experimental values.

The overall principle of coupling an external circuit to the PIC/MCC model is given in Ref. 7. Verboncoeur *et al.*[8] and Lawson[9] treated the general one-dimensional (1D) case, and van der Straaten[10] treated the 1D case applied to a cylindrical magnetron. Vahedi *et al.* studied the general two-dimensional (2D) Cartesian case.[11,12] However, there exists

a)Electronic mail: evi.bultinck@ua.ac.be.

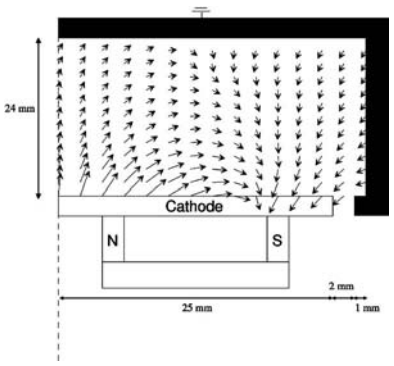

FIG. 1. Scheme of the magnetron with the magnetic field vectors indicated. For symmetry reasons, only half of the reactor is shown (the dashed vertical line represents the symmetry axis).

no PIC/MCC model yet in 2D cylindrical geometry with external circuit included, beside the work of Kolev *et al.*[3,13–15] Therefore, in the present paper we explain how this external circuit is implemented. The implementation is based on the earlier mentioned research, but the necessary modifications were done for the 2D cylindrical geometry. Furthermore, we investigate the importance of including an external circuit in a PIC/MCC dc magnetron code by comparing it with results when an external circuit is not included.

II. DESCRIPTION OF THE MAGNETRON UNDER STUDY

The scheme of the planar magnetron investigated in the present study is given in Fig. 1. It is based on the magnetron used in the experiments described in Ref. 16. An electric field is generated by connecting a dc power supply to the powered electrode (the cathode). The other walls are grounded and thereby act as an anode. An axisymmetric magnetic field is created by two concentric magnets located beneath the cathode. The magnetron is balanced, meaning that the majority of the magnetic flux lines that originate at the cathode, also return to the cathode without crossing the anode. The radius of the cathode is 25 mm, the gap between the cathode and the closest wall is 2 mm, and the distance between the cathode and the opposite anode is 24 mm.

In our simulations, we assume that the magnetron operates in pure argon and at room temperature (300 K).

III. DESCRIPTION OF THE MODEL

A. General overview of the model

The model used in the present work is a 2d3v PIC/MCC model. The details of this method are given in Refs. 3, 7, and 13–15. The flow chart of the model is given in Fig. 2.

The real particles in the discharge are represented by a limited ensemble of so-called superparticles (SPs). Each SP represents W real particles, where W is known as the weight. The program starts with initial densities of the electrons and Ar^+ ions, i.e., 10^{15} m^{-3}. The initial number of electron and Ar^+ SPs is 90 000. Initially, the SPs are uniformly distributed and are assumed to have Maxwellian velocities. The SPs move in each time step (electron SPs move each 4×10^{-11} s, ion SPs every 20th electron time step, see Sec. III D) due to the external magnetic and electric field and the electric field generated by the SPs themselves (see later). Their positions and velocities are calculated according to Newton's equations of motion

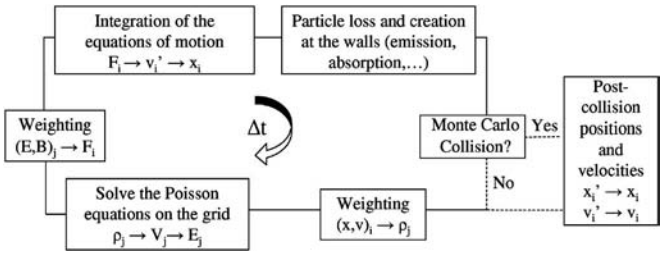

FIG. 2. Flow chart of the PIC/MCC model. The subscript i denotes the particle quantities and j denotes the grid quantities.

$$m\frac{d\mathbf{v}}{dt} = q(\mathbf{E} + \mathbf{v}\times\mathbf{B}),$$
$$\frac{d\mathbf{x}}{dt} = \mathbf{v}, \tag{1}$$

where m is the mass, $\mathbf{v}$ is the velocity, q is the charge, $\mathbf{x}$ is the position, $\mathbf{E}$ is the electric field, and $\mathbf{B}$ is the magnetic field. These equations are discretized using the central finite difference method. To achieve this, the so-called leap-frog method is used.[7] The $\mathbf{v}\times\mathbf{B}$ rotation term is treated according to the algorithm suggested by Boris.[17]

The particles collide in the MCC module. At the middle of the time step, the probability of the kth collision type is

$$P^k = 1 - \exp[-\Delta s n_{\text{tar}}\sigma_k(E_i)], \tag{2}$$

with n_{tar} the density of the target species and $\sigma_k(E_i)$ is the collision cross section as a function of the energy of the incident particle E_i. This probability is compared to a random number, uniformly distributed in the interval $[0,1]$. If this random number is smaller, then the collision takes place, and the particles receive new positions and velocities according to the collision type. Details about their treatment are given in Refs. 13 and 14. The list of the considered collisions and their corresponding cross sections is given in Table I. Coulomb collisions are not included because of the low degree of ionization.[13,18] The sputtered atoms from the cathode are not included in the model either since their contribution to the current problem is not important. Indeed, we want to investigate the influence of the external circuit on the cathode current, which is only dependent on charged particles and not

TABLE I. List of the considered collisions and their corresponding cross sections.

$e^- + Ar \rightarrow e^- + Ar$	Elastic scattering	Ref. 31
$e^- + Ar \rightarrow 2e^- + Ar^+$	Electron-impact ionization	Ref. 32
$e^- + Ar \rightarrow e^- + Ar_m^*$	Electron-impact excitation	Ref. 33
$e^- + Ar \rightarrow e^- + Ar^*$	Electron-impact excitation	Ref. 34
$Ar^+ + Ar \rightarrow Ar^+ + Ar$	Elastic scattering	Ref. 35
$Ar^+ + Ar \rightarrow Ar + Ar^+$	Charge transfer	Ref. 35
$Ar^+ + Ar \rightarrow 2Ar^+ + e^-$	Ion-impact ionization	Ref. 36
$Ar^+ + Ar \rightarrow Ar^+ + Ar_m^*$	Ion-impact excitation	Ref. 36

on neutral sputtered particles. Also, the contribution of the ionized sputtered particles is not very significant to the charge density.[14]

The term "particle-in-cell" refers to the weighting of the SPs to a grid.[7] The earlier mentioned particle quantities are calculated on the particles themselves; the field quantities, however, are obtained on a spatial grid. Therefore, a first-order weighting scheme[7] is used to achieve a charged particle density landscape on the grid. The electrical potential V is calculated from this charge density using the Poisson equation in (r,z) coordinates

$$\frac{1}{r}\frac{\partial}{\partial r}r\frac{\partial V}{\partial r}+\frac{\partial}{\partial z}\frac{\partial V}{\partial z}=-\frac{q}{\epsilon_0}(n_i-n_e), \tag{3}$$

with q as the elementary charge, ϵ_0 as the dielectric constant, and n_i and n_e as the ion and electron densities, respectively. In order to simplify the solution of this equation, we use the superposition principle, so that the electrical potential can be presented as the sum of the potential only due to the space charge (V_P) and the potential only due to the cathode voltage (U_0),

$$V=V_P+U_0V_L, \tag{4}$$

where V_L is the dimensionless potential due to an applied voltage with magnitude 1 V.[12] V_P can be found as a solution of Eq. (3) with zero potential boundary conditions, i.e., $V_P=0$ at the surfaces $z=0$, $z=z_{\max}$, and $r=r_{\max}$. Due to the cylindrical symmetry, the physical boundary condition at $r=0$ is

$$\left(\frac{\partial V_P}{\partial r}\right)_{r=0}=0. \tag{5}$$

V_L is the solution of the Laplace equation

$$\Delta V_L=0, \tag{6}$$

with the applied potential boundary condition, i.e., $V_L=1$ at the cathode surface and $V_L=0$ at the grounded walls. Moreover, in the gap between the cathode and the grounded wall at $z=0$, V_L is assumed to decay linearly from 1 to 0 with the distance from the cathode. The Laplace equation needs to be solved only at the beginning of the simulation which simplifies and accelerates the calculation of the Poisson equation. Equations (3) and (6) are discretized using a standard five-point stencil[19] and solved on a grid with $\Delta r=0.5$ mm and $\Delta z=0.1$ mm. The electric field E is obtained as

$$\mathbf{E}=-\nabla V. \tag{7}$$

This equation is discretized by the central finite difference method. On the boundaries, forward or backward differencing is applied. This new electric field, together with the applied electric and magnetic field, moves the particles again during the next time step and the procedure is repeated.

B. Description of the external circuit

1. Justification

The critical value of the potential needed for a gas to breakdown into a partially ionized gas is called the breakdown voltage (V_b).[20] If this voltage is reached across the electrodes, a self-sustaining discharge begins to burn in the gas. The formation of charged particles induces a current to flow in the plasma. This current grows, and in the idealized case, tends to infinity.[20]

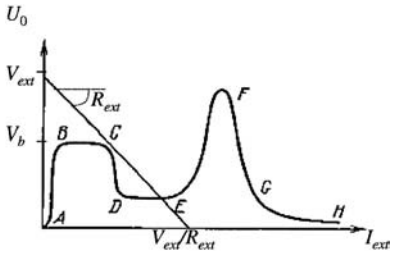

FIG. 3. General voltage–current characteristics of gas discharges. The diagonal straight line is the so-called load line, which represents the following equation: $V_{ext}=U_0+R_{ext}I_{ext}$, where U_0 is the voltage drop between the electrodes, I_{ext} is the current in the external circuit, R_{ext} is the external constant resistance, and V_{ext} is the external constant voltage (Ref. 20).

The discharge current can be plotted against the voltage between the electrodes; the $V-I$ characteristic for a nonmagnetized discharge is shown in Fig. 3.[20] Certain areas can be distinguished according to the discharge current. A–B $(10^{-10}-10^{-9}$ A) is the region of a nonself-sustaining discharge, B–C $(10^{-9}-10^{-5}$ A) corresponds to a Townsend discharge, D–E $(10^{-4}-10^{-1}$ A) is a normal glow discharge, E–F $(10^{-1}-1$ A) is an abnormal glow discharge, F–G $(1-10$ A) is the transition to arcing, and G–H $(10^{-10}$ A$-\ldots)$ is the region of an arc discharge. These are well-known values for the nonmagnetized discharge, but unfortunately, no research is done for the magnetized discharge. However, we use these values to evaluate the calculated current regime.

As is clear from Fig. 3, there are areas where more than one current corresponds to a given voltage. The reason for that are regimes with a negative differential resistance, meaning that the current increases with decreasing voltage (for example C–D and F–G on Fig. 3).

Any real circuit combined with a discharge gap contains an ohmic resistance; a specially introduced one, or simply the resistance of the wires of the power source. If a constant resistor, R_{ext}, and a constant voltage source, V_{ext}, are connected in series to a discharge gap (Fig. 4), the Kirchhoff's voltage loop law is

$$V_{ext}=U_0+R_{ext}I_{ext}. \tag{8}$$

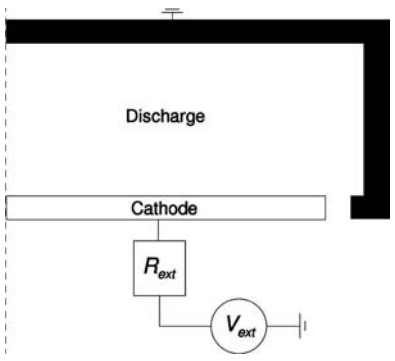

FIG. 4. Scheme of the external circuit connected to the discharge. R_{ext} represents the external resistance and V_{ext} represents the external voltage.

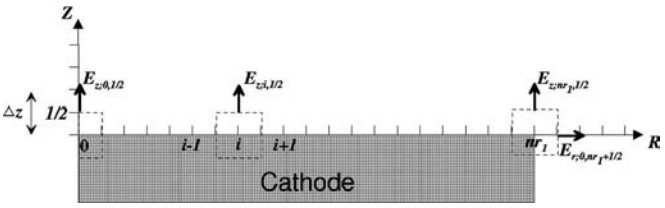

FIG. 5. The Gauss' theorem on a box surrounding the cathode.

In Sec. III B 2, it will be shown how the voltage drop between the electrodes (U_0) can be calculated and the current in the external circuit (I_{ext}) can be obtained from Eq. (8). This equation is plotted as a straight line, the so-called load line, in U_0 versus I_{ext} coordinates, as seen in Fig. 3, and the intercept on the x axis is the limiting current $V_{\text{ext}}/R_{\text{ext}}$. This load line determines the discharge current regime (where the load line crosses the curve) and therefore the type of discharge. In other words, the type of discharge and the discharge current regime are determined by the external resistance and voltage.

The importance of the external circuit is therefore to limit the current to a certain regime. This implies that neglecting this circuit may cause the current to converge to a wrong voltage–current regime, or even diverge to infinity.

2. Coupling of the external circuit to the PIC/MCC code

As explained earlier, a current-limiting mechanism is inevitable in the operation of gas discharges. Obviously, this statement also holds for the modeling of magnetrons. The simplest external circuit consists of a ballast resistor R_{ext} and a constant voltage source V_{ext} in series with the cathode (Fig. 4).

In the presence of an external circuit, the cathode potential is a function of both the discharge process and the external parameters. Simultaneous advance in time of the simulation of the discharge and the circuit is necessary, leading to a complete coupling of the discharge and the external circuit. This coupling is maintained by satisfying the charge conservation at the cathode[11]

$$A\frac{d\sigma}{dt} = I_{\text{ext}}(t) + AJ_{\text{dis}}, \tag{9}$$

where A is the cathode area, σ its total surface charge density, I_{ext} is the current in the external circuit, and J_{dis} is the current density arriving at the cathode due to the charged plasma species.

The surface charge can be determined independently of Eq. (9) applying the Gauss' theorem on a box surrounding the cathode (see Fig. 5)[11]

$$\oint_{S_i} \epsilon_0 \mathbf{E}\cdot d\mathbf{S} = \oint_{S_i} \sigma_i d\mathbf{S} + \int_{Vol_i} \rho_i dV = Q_i. \tag{10}$$

Here, σ_i is the surface charge density at point i on the cathode surface, ρ_i is the volume charge density in the same point, and Q_i the total charge inside the box.

Similar to the procedure applied in Ref. 11, Eq. (10) is equivalent to[21]

$$\epsilon_0 E_{z;i,1/2} S_i = \sigma_i S_i + \tfrac{1}{2}\rho_i \text{Vol}_i. \tag{11}$$

$E_{z;i,1/2}$ is the electric field in the z direction in point $(i,1/2)$. S_i is the surface of the box around point i and Vol_i is its volume, which is equal to $S_i\Delta z$ with Δz the grid size in the z direction. From Fig. 5, it is clear that only half of the volume contributes to the charge density in Vol_i, which declares the factor $1/2$.

Using central finite differencing, $E_{z;i,1/2}$ can be expressed as $(U_0 - V_{i,1})/\Delta z$, where U_0 is the cathode potential and $V_{i,1}$ is the potential in the first grid point of the discharge region. The cathode is assumed to be a perfect conductor, meaning that there is no radial dependence of the cathode potential. Equation (11) can then be rewritten similar to Ref. 11 and yields for σ_i (Ref. 21)

$$\begin{aligned}
\sigma_i &= \frac{\epsilon_0}{\Delta z}U_0 - \frac{\epsilon_0}{\Delta z}V_{i,1} - \frac{\Delta z}{2}\rho_i \quad i \in [0, nr_1 - 1], \\
\sigma_{nr_1} &= \left(\frac{\epsilon_0}{\Delta z}C_1 + \epsilon_0 C_2\right)U_0 - \frac{\epsilon_0}{\Delta z}C_1 V_{nr_1,1} - C_3\rho_{nr_1,0},
\end{aligned} \tag{12}$$

with constants C_1, C_2, and C_3,

$$\begin{aligned}
C_1 &= \frac{r_{nr_1}^2 - r_{nr_1-1/2}^2}{r_{nr_1}^2 - r_{nr_1-1/2}^2 + r_{nr_1}\Delta z}, \\
C_2 &= \frac{1}{r_{nr_1+1/2} - r_{nr_1-1/2}} \frac{r_{nr_1+1} - r_{nr_1}}{r_{nr_2} - r_{nr_1}} \frac{r_{nr_1}\Delta z}{r_{nr_1}^2 - r_{nr_1-1/2}^2 + r_{nr_1}\Delta z}, \\
C_3 &= \frac{\Delta z}{2}\frac{2r_{nr_1+1/2}^2 - r_{nr_1}^2 - r_{nr_1-1/2}^2}{r_{nr_1}^2 - r_{nr_1-1/2}^2 + r_{nr_1\Delta z}}.
\end{aligned} \tag{13}$$

The total surface charge on the cathode is the sum of the surface charge densities in all the cells

$$\sigma_T = \sum_{i=0}^{nr_1} \sigma_i = \sum_{i=0}^{nr_1-1} \sigma_i + \sigma_{nr_1}. \tag{14}$$

This yields for the total cathode surface charge[21]

$$\sigma_T = a_1 U_0 + a_2 \sum_{i=0}^{nr_1-1} V_{i,1} + a_3 V_{nr_1,1} + a_4 \sum_{i=0}^{nr_1-1} \rho_{i,0} + a_5 \rho_{nr_1,0}, \tag{15}$$

with

$$\begin{aligned}
a_1 &= nr_1\frac{\epsilon_0}{\Delta z} + \frac{\epsilon_0}{\Delta z}C_1 + \epsilon_0 C_2, \\
a_2 &= -\frac{\epsilon_0}{\Delta z}, \\
a_3 &= a_2 C_1, \\
a_4 &= -\frac{\Delta z}{2}, \\
a_5 &= -C_3.
\end{aligned} \tag{16}$$

On the other hand, Eq. (9) can be discretized with the backward finite difference method (backward, because we have information about the surface charge of the previous time step)

$$A(\sigma_T^t - \sigma_T^{t-1}) = [I_{\text{ext}}(t) + AJ_{\text{dis}}]\Delta t. \tag{17}$$

Using Eq. (8) for an expression of I_{ext}, Eq. (17) leads to

$$\sigma_T^t = \frac{1}{A}(V_{\text{ext}} - U_0)\frac{\Delta t}{R_{\text{ext}}} + J_{\text{dis}}\Delta t + \sigma_T^{t-1}. \tag{18}$$

Equations (15) and (18) can then be combined in one equation to obtain an expression for the cathode potential U_0. The problem with this expression is that $V_{i,1}$ depends on both the discharge and the boundary. This implies that the expression is a boundary condition for the Poisson equation, meaning that the Poisson equation must be solved iteratively until the boundary condition is fulfilled. This obviously requires a long calculation time and is computationally very inefficient. Alternatively, the potential $V_{i,j}$ can be expressed with the superposition principle [see also Eq. (4) earlier][11]

$$V_{i,j} = V_{i,j}^P + U_0 V_{i,j}^L. \tag{19}$$

Combining Eqs. (15) and (18) and replacing $V_{i,j}$ with Eq. (19) leads to an expression of the cathode potential U_0,[21]

$$U_0 = \frac{-a_2\Sigma_{i=0}^{nr_1-1}V_{i,1}^P - a_3V_{nr_1,1}^P - a_4\Sigma_{i=0}^{nr_1-1}\rho_{i,0} - a_5\rho_{nr_1,0} + J_{\text{dis}}\Delta t + a_6V_{\text{ext}} + \sigma_T^{t-1}}{a_7}, \tag{20}$$

where

$$a_6 = \frac{\Delta t}{R_{\text{ext}}A},$$
$$a_7 = a_1 + a_2\sum_{i=0}^{nr_1-1}V_{i,1}^L + a_3V_{nr_1,1}^L - a_6. \tag{21}$$

In this way, U_0 is calculated self-consistently from the potentials $V_{i,1}^P$ and $V_{i,1}^L$, the volume charge density $\rho_{i,0}$ (at all points i on the cathode surface), the current density of the charged plasma species to the cathode J_{dis}, the cathode surface charge from the previous time step σ_T^{t-1}, and the time step itself (Δt), and from the constants V_{ext}, R_{ext} and the geometric parameters of the grid. The external current I_{ext}, which is equal to the plasma current at steady state, can be calculated from Eq. (8).

C. Reflection coefficient and secondary electron emission coefficient

Due to the low pressure and the magnetic field a significant number of secondary electrons have the ability to return to the cathode.[13,22] When this happens, they can be reflected or absorbed depending on the reflection coefficient (RC), given as the number of electrons that are reflected back in the discharge versus the number of incident electrons, and which is thus given by a value between 0 and 1. It is shown that this recapture of secondary electrons has a great effect on the discharge characteristics.[13] Consequently, the RC also has a great effect on the calculated cathode potential and current, which is of considerable interest in this study. The more electrons are absorbed at the cathode, the more negative is the cathode potential and the lower (less positive) is the cathode current. It is shown that a change in RC of 0–0.5 results in a decrease (in absolute value) of the cathode potential of approximately 30 V.[13] Unfortunately, experimental values for the RC are very scarce, making the RC a very delicate parameter in simulating magnetron discharges. However, the cathode potential and current can be both calculated and measured very accurately, so the RC can be used as a fitting parameter for the calculated cathode potential and current to be compared to the measured value[13] if an external circuit is included (because neglecting the external circuit will give rise to wrong cathode currents).

Furthermore, the secondary electron emission coefficient (SEEC), given as the number of secondary electrons produced by an ion striking the cathode, also plays an important role in the discharge characteristics. Therefore, analogous to the RC, the SEEC also has a great effect on the calculated cathode potential. Unfortunately, the SEEC is also extremely hard to measure. Therefore, it is also used as fitting parameter for the calculation of the cathode potential. However, its value is only varied within a range of realistic values,[23–27] so that it still has a physical meaning. If the SEEC is taken too large, it is shown that calculations without an external circuit will even not converge due to an unbounded increase of SP.[6]

D. Additional remarks

There are a few more aspects that are worth mentioning about the time step and speeding up the simulation. To avoid instability of the simulation, the time step is limited by two criteria: the stability and the Courant criterion.[7,13]

To speed up the simulation, the electron time step is taken much smaller than the ion time step. Ions are moved only once per 20 electron time steps because electrons are much faster due to their lower mass. After every ion time step, the number of superparticles is counted, and, if increased above a predefined limit, reduced twice. Correspondingly, the weight of the remaining superparticles is doubled.[15]

Another manner to speed up the code is to sort the SPs. Details on the sorting algorithm are given in Ref. 28.

IV. RESULTS AND DISCUSSION

As shown in Fig. 3, several voltage–current regimes exist in discharges. Logically every regime has its own discharge characteristics. In the present paper, two regimes were studied in the magnetron, namely the normal glow discharge and the abnormal glow discharge regime. As mentioned before, only the calculations with external circuit can bring the discharge in a desired regime.

A. The "normal glow discharge" regime

In order for the discharge to operate in the normal glow discharge regime, the external voltage must be low and the external resistance high (see Fig. 3). The following input values were used for the external potential, external resistance, gas pressure, RC, and SEEC: −400 V, 1500 Ω, 1.0 Pa, 0.1, and 0.07. The calculations are run until convergence of the cathode potential, typically after around 20 μs. The cathode potential at steady state of the plasma was calculated to be −272 V. The cathode current was calculated as 0.086 A, which corresponds to regime D–E on Fig. 3.

We have studied the effect of the cathode current on the discharge characteristics in this normal glow discharge regime. This was achieved by varying the external resistance. The following values were used: 1500, 2000, and 2500 Ω.

When the resistance is increased, the external current decreases, also causing a drop of the cathode current. The calculated cathode currents for the given resistances are 0.086, 0.063, and 0.048 A, respectively. These currents also correspond to the D–E regime at Fig. 3, what causes the cathode potential to be nearly constant. Indeed, the calculated values for the cathode potential for the given resistances are −272, −274, and −281 V, respectively. The small increase in cathode potential could refer to an area of slightly negative differential resistance, causing the voltage drop $R_{ext}I_{ext}$ to decrease with increasing resistance. From Eq. (8), it is clear that this causes the cathode potential to increase (i.e., become more negative). Indeed, at the low current regime, the secondary electrons play the most important role in sustaining the discharge. These secondary electrons can return to the cathode in their magnetic traps. In this way, they provide a more negative charge for the cathode, and as a result, the cathode potential will increase slightly (i.e., become more negative).

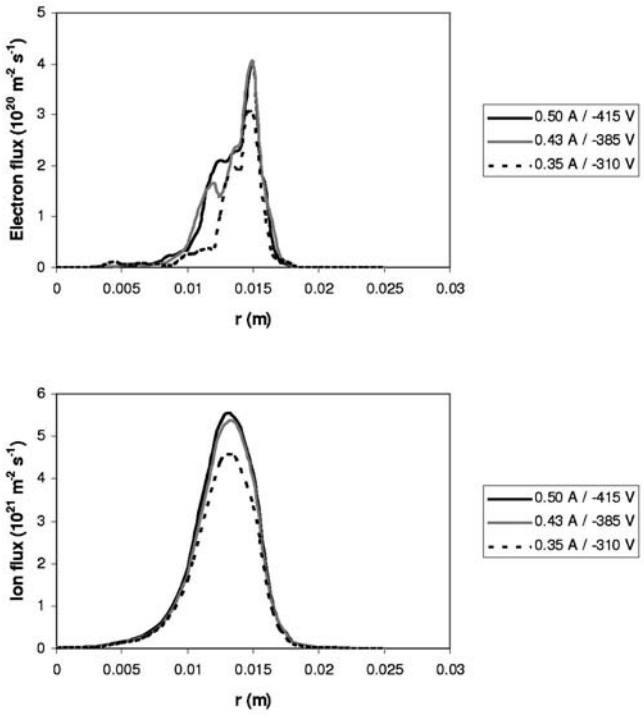

FIG. 6. Calculated electron flux (a) and Ar^+ flux (b) at a constant pressure of 1.0 Pa and three different values of cathode current and potential in the abnormal glow discharge regime. For symmetry reasons, only half of the cathode is presented.

TABLE II. Measured and calculated values of the cathode currents and corresponding potentials for a pressure of 1.0 Pa.

Measured		Calculated	
Current (A)	Potential (V)	Current (A)	Potential (V)
0.2	−336.4	0.35	−310
0.4	−382.5	0.43	−385
0.6	−405.1	0.50	−415

B. The "abnormal glow discharge" regime

Because most magnetron experiments operate at higher currents (typically 0.1−1 A),[29] i.e., regime E–F on Fig. 3, we have adjusted the earlier mentioned input to force the cathode current into the E–F regime. This allows us to verify the calculation with experimental values.[30] To reach this regime, the external voltage is increased and the external resistance is decreased so that the load line shifts to a higher limiting current.

The input values used were an external potential of −468.7 V and a gas pressure of 1.0 Pa.[30] To study the effect of the cathode current, the external resistance was varied over 500, 200, and 100 Ω.

To verify the calculated results, we have compared them with experimental data, performed by Heirwegh,[30] as shown in Table II. For the earlier mentioned values of the external resistance, a RC of 0.3 and a SEEC of 0.07 were used to obtain the calculated values for the cathode current and potential, as summarized in Table II as well. From Table II, we can conclude that a good agreement is reached between the calculations and the experimental values. A higher cathode potential results in a higher current, as expected. Therefore, all the other calculated plasma characteristics are more likely to be correct, such as charged particle fluxes and densities, and plasma potential distribution, which are relatively hard to measure.

The trends of the calculated currents and potentials are also manifested in the particle fluxes. An increased resistance, leading to a lower current and potential, causes a decrease in the particle fluxes (shown in Fig. 6). The characteristic profile of the charged particle fluxes is caused by the magnetic field that traps the electrons near the cathode. Indeed, the maximum of the electron and ion flux is due to the fact that the radial magnetic field is highest here (see Fig. 1).

This leads to a trapping of the electrons. Therefore, the electrons cause most ionizations here, leading to a maximum ion density close to the cathode. This causes the maximum of the fluxes to be situated here. However, a slight shift of the maximum of the electron flux can be noticed, but it is considered as not significant. Obviously, the ion flux is an order of magnitude larger than the electron flux because the electric field causes an attraction of ions and a repulsion of electrons, leading to a lower electron flux compared to the ion flux. This ion flux causes the typical race track area on the cathode surface of a magnetron discharge, i.e., the region where most particles are sputtered from the cathode.

The lower current causes the charged particle densities to decrease as well (as is seen in Fig. 7, where the electron density is presented). (The ion density is similar, so it is not shown here.) The electrons and ions are well localized near the cathode. This is also a consequence of the magnetic field and the resulting enhanced ionization (see earlier).

It is obvious that there are great differences between the normal and abnormal glow discharge regime. Besides the difference in potential-current dependence, the abnormal regime operates at higher currents, causing all the other plasma characteristics, for example, charged particle fluxes and densities, to be larger. Indeed, the charged particle fluxes and densities in the abnormal regime were calculated to be almost one order of magnitude larger than in the normal regime.

C. Comparison with and without external circuit

To investigate the importance of the external circuit in our calculations, we have carried out a comparison of the model with and without external circuit.

When working without an external circuit, it appears that an appropriate choice of the input values such as pressure, potential, current, RC, and SEEC is very important to avoid either divergence of the cathode current or a zero cathode current. Calculations were performed for pressures in the range of 0.4–1.0 Pa and potentials received from Heirwegh,[30] but only a limited number of combinations yielded converged results. From the difficulty to reach convergence, it is obvious that a simulation without external circuit is very sensitive to changes of any input value in terms of stability of the code. In contrast, the stability of the code in simulations with the external circuit included is not at all sensitive to changing the input values. That is one reason why an external circuit is inevitable in a PIC/MCC simulation of every kind of discharge, among which magnetrons.

Another reason is that in the rare case that a calculation without external circuit converges, the results are not at all reliable because the calculated current is either zero or is a few orders of magnitude too low. This will be shown in Secs. IV C 1 and IV C 2. Indeed, it was shown that only the calculations with external circuit are comparable with experimental values, as seen in Sec. IV B.

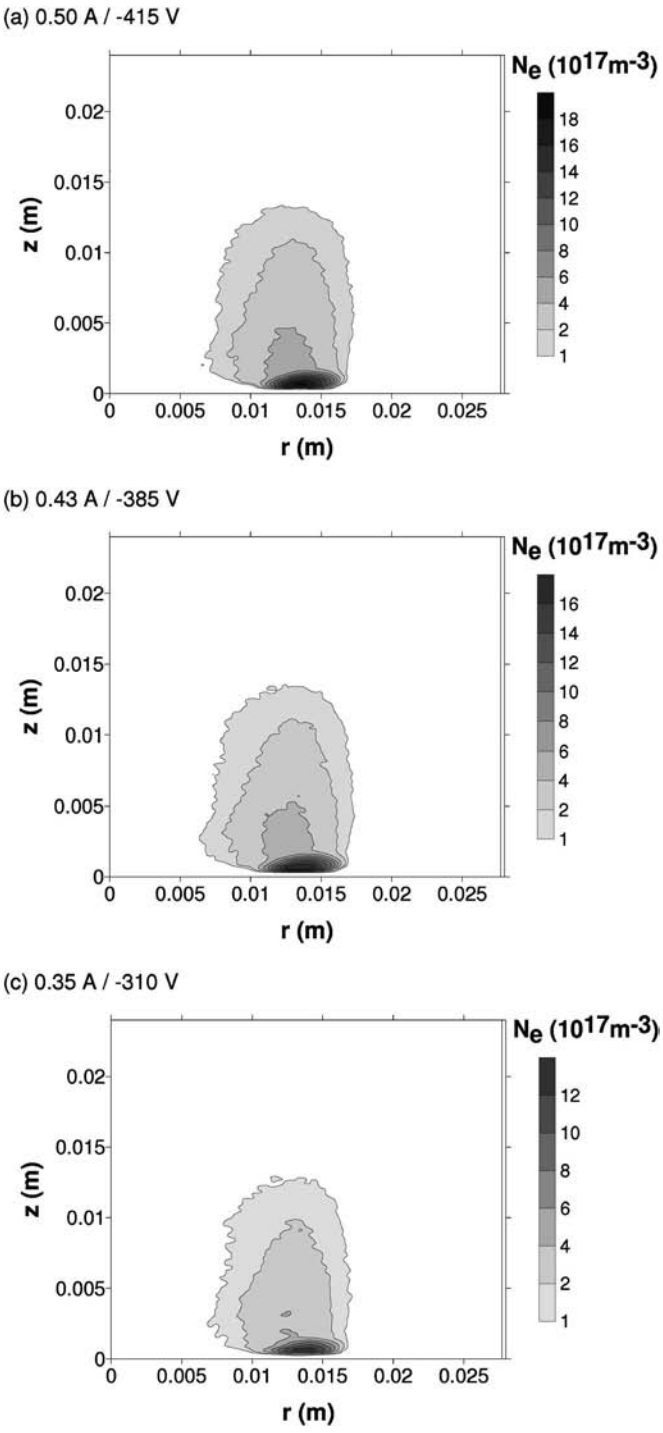

FIG. 7. Calculated electron densities at a constant pressure of 1.0 Pa and three different values of cathode potential and current in the abnormal glow discharge regime. For symmetry reasons, only half of the cathode is presented.

1. In the normal glow discharge regime

For a typical input set of the normal glow discharge regime, namely a pressure of 1.0 Pa, an external potential of −400 V, an external resistance of 1500 Ω, a RC of 0.1, and a SEEC of 0.07, the cathode potential at steady state of the plasma was calculated to be −272 V in the model with external circuit included (see Sec. IV A). To emphasize the importance of the external circuit, attempts were made to compare the results of a simulation with external circuit to

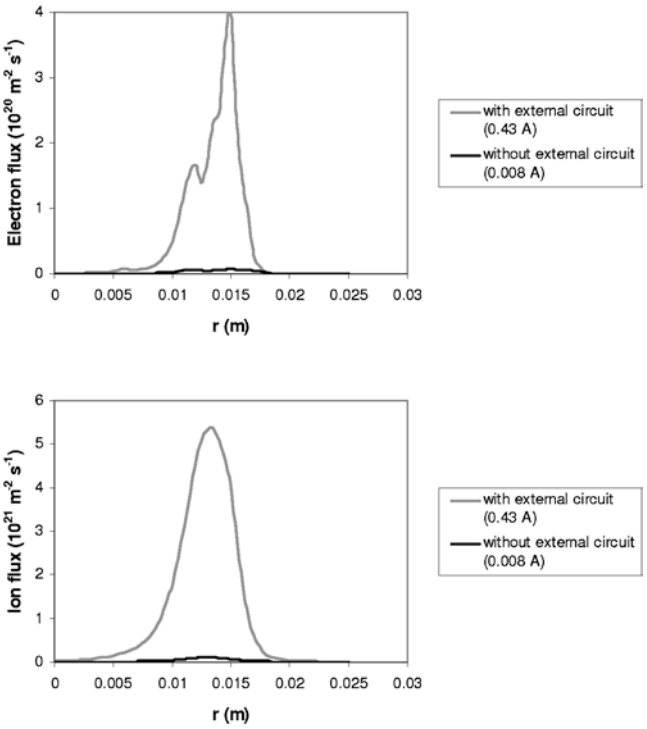

FIG. 8. (Color online) Calculated electron flux (a) and Ar^+ flux (b) at a constant pressure of 1.0 Pa obtained with and without including the external circuit. For symmetry reasons, only half of the cathode is presented.

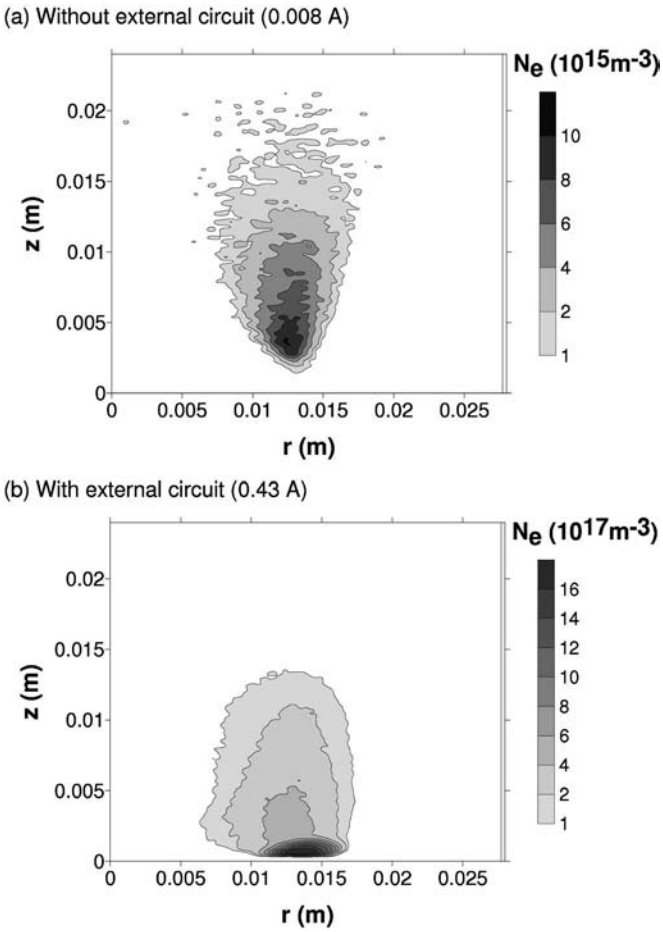

FIG. 9. Calculated electron densities at a constant pressure of 1.0 Pa obtained with and without including the external circuit. For symmetry reasons, only half of the cathode is presented.

those without external circuit. In order for this comparison to be meaningful, the cathode potential of this converged simulation should be used as input for the calculation without external circuit, instead of calculating it self-consistently when working with an external resistance and potential, as explained in Sec. III B. Using the cathode potential as input is the common procedure when neglecting the external circuit to study the plasma quantities (e.g., Refs. 4–6).

Unfortunately, the calculated cathode potential of −272 V appeared too low to get convergence: the cathode current of the simulation without external circuit became zero (i.e., the discharge extinguishes), whereas the cathode current with external circuit was calculated as 0.086 A (see Sec. IV A). This implies that an external circuit is necessary in a PIC/MCC simulation because using the same input values but omitting an external circuit leads to a different result than with external circuit, namely to a zero cathode current.

2. In the abnormal glow discharge regime

For a typical input set of the abnormal glow discharge regime, namely a pressure of 1.0 Pa, an external potential of −468.7 V, an external resistance of 200 Ω, a RC of 0.3, and a SEEC of 0.07, the cathode potential at steady state of the plasma was calculated to be −385 V (see Sec. IV B). This cathode potential is again used as input for the calculation without external circuit in order to be able to compare the results.

As seen in Sec. IV B, the measured cathode current for the earlier mentioned input values is 0.4 A. Hence, there is a good agreement with the calculated value of 0.43 A. The cathode current, calculated with the same input values in a code without external circuit, however, was calculated as 0.008 A. This means that neglecting an external circuit causes the cathode current to converge to a value which is almost two orders of magnitude too low.

Figure 8 illustrates the calculated charged particle fluxes with and without external circuit included. It is clear that the fluxes are a few orders of magnitude lower without than with external circuit. The charged particle densities follow this trend, as shown in Fig. 9, for the electron density. The calculated electron density with external circuit is not only two orders of magnitude larger, but the profile is also totally different, i.e., the maximum of the electron density is located closer to the cathode. This is because the sheath narrows when an external circuit is included, presented in Fig. 10. Indeed, because of the higher electron density, more ionization takes place, so that the sheath can be thinner to sustain the discharge.

The large differences in plasma characteristics are a direct consequence of the wrong calculated current when an external circuit is neglected.

V. CONCLUSION

A plasma can be formed in many different voltage–current ($V-I$) regimes, and all of them have their own plasma characteristics. An external circuit can force the dis-

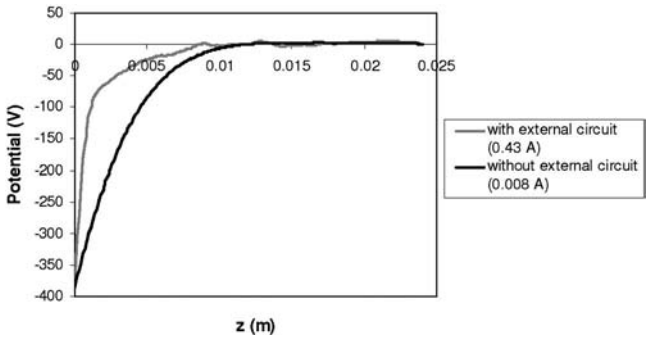

FIG. 10. Calculated potential distribution at a line above the race track (i.e., $r=0.013$ m) at a constant pressure of 1.0 Pa obtained with and without including the external circuit.

charge into a certain regime by modifying the external voltage and resistance. This was demonstrated by calculations for a normal glow discharge and an abnormal glow discharge regime of a dc magnetron discharge. The calculated results from the "abnormal" regime were validated by experiment.[30]

In a model without external circuit, on the other hand, the calculated current will not be limited, leading to stability problems, or, in a small number of cases, to a converged current, which is most likely in a wrong $V-I$ regime. We have shown that the calculated current is indeed a few orders of magnitude too low when neglecting the external circuit, causing the calculated plasma characteristics to be too low.

The overall conclusion is that an external circuit is inevitable in a PIC/MCC code for an accurate and correct description of magnetron discharges, and in general, of all dc glow discharges.

ACKNOWLEDGMENTS

E. Bultinck is indebted to the Institute for the Promotion of Innovation by Science and Technology in Flanders (IWT Flanders) for financial support. The authors would like to thank S. Heirwegh for the interesting discussions and the provided experimental data. Also, the authors thank Z. Donko for the enlightening help on the external circuit. Finally, the authors thank R. Gijbels for the interesting discussions in general.

[1] R. K. Waits, J. Vac. Sci. Technol. **15**, 179 (1978).
[2] J. W. Bradley, S. Thompson, and Y. A. Gonzalvo, Plasma Sources Sci. Technol. **10**, 490 (2001).
[3] I. Kolev and A. Bogaerts, Contrib. Plasma Phys. **44**, 582 (2004).
[4] K. Nanbu, K. Mitsui, and S. Kondo, J. Phys. D **33**, 2274 (2000).
[5] C. H. Shon and J. K. Lee, Appl. Surf. Sci. **192**, 258 (2002).
[6] Y. Kusumoto and K. Iwata, Vacuum **74**, 359 (2004).
[7] C. K. Birdsall and A. B. Langdon, *Plasma Physics via Computer Simulations* (IOP, Bristol, 1991).
[8] J. P. Verboncoeur, M. V. Alves, V. Vahedi, and C. K. Birdsall, J. Comput. Phys. **104**, 321 (1993).
[9] W. S. Lawson, J. Comput. Phys. **80**, 253 (1989).
[10] T. A. van der Straaten, N. F. Cramer, I. S. Falconer, and B. W. James, J. Phys. D **31**, 177 (1998).
[11] V. Vahedi and G. DiPeso, J. Comput. Phys. **131**, 149 (1997).
[12] V. Vahedi, C. K. Birdsall, M. A. Lieberman, G. DiPeso, and T. D. Rognlien, Phys. Fluids B **5**, 2719 (1993).
[13] I. Kolev, A. Bogaerts, and R. Gijbels, Phys. Rev. E **72**, 056402 (2005).
[14] I. Kolev and A. Bogaerts, IEEE Trans. Plasma Sci. **34**, 886 (2006).
[15] I. Kolev and A. Bogaerts, Plasma Processes Polym. **3**, 127 (2006).
[16] D. Depla, G. Buyle, J. Haemers, and R. D. Gryse, Surf. Coat. Technol. **200**, 4329 (2006).
[17] *Relativistic Plasma Simulation—Optimization of a Hybrid Code*, Fourth Conference on the Numerical Simulation of Plasma (Naval Research Laboratory, Washington, DC, 1970), Vol. 3, pp. 3–67.
[18] G. Buyle, Ph.D. thesis, Ghent University, 2005.
[19] F. S. Acton, *Numerical Methods That Work* (Mathematical Association of America, Washington, 1991).
[20] Y. R. Raizer, *Gas Discharge Physics* (Springer, Berlin, 1991).
[21] I. Kolev, Ph.D. thesis, University of Antwerp, 2007.
[22] G. Buyle, D. Depla, K. Eufinger, and R. D. Gryse, J. Phys. D **37**, 1639 (2004).
[23] M. A. Lewis, D. A. Glocker, and J. Jorne, J. Vac. Sci. Technol. A **7**, 1019 (1989).
[24] P. C. Smith, B. Hu, and D. N. Ruzic, J. Vac. Sci. Technol. A **12**, 2692 (1994).
[25] L. M. Kishinevsky, Radiat. Eff. **19**, 23 (1973).
[26] R. A. Baragiola, E. V. Alonso, J. Ferron, and A. Olivaflorio, Surf. Sci. **90**, 240 (1979).
[27] R. A. Baragiola, *Inelastic Particle-Surface Collisions* (Springer, Berlin, 1981).
[28] K. J. Bowers, J. Comput. Phys. **173**, 393 (2001).
[29] G. Y. Yeom and J. A. Thornton, J. Appl. Phys. **65**, 3816 (1989).
[30] S. Heirwegh, private communication.
[31] M. Hayashi, unpublished, online available: ftp://jila.colorado.edu/collision_data/electronneutral/hayashi.txt.
[32] A. V. Phelps and Z. L. Petrovic, Plasma Sources Sci. Technol. **8**, R21 (1999).
[33] N. J. Mason and W. R. Newell, J. Phys. B **20**, 1357 (1987).
[34] E. Eggarter, J. Chem. Phys. **62**, 833 (1975).
[35] A. V. Phelps, J. Appl. Phys. **76**, 747 (1994).
[36] A. V. Phelps, J. Phys. Chem. Ref. Data **20**, 557 (1991).